Hindawi
Mathematical Problems in Engineering
Volume 2022, Article ID 9982817, 12 pages
https://doi.org/10.1155/2022/9982817

Research Article

Direct Position Determination of Noncircular Sources with Multiple Nested Arrays via Weighted Subspace Data Fusion

Yang Qian[1,2], **Xinlei Shi**[1,2], **Haowei Zeng**[1,2] and **Xudong Dong**[1,2]

[1]*College of Electronic Information Engineering, Nanjing University of Aeronautics and Astronautics, Nanjing 211106, China*
[2]*Key Laboratory of Dynamic Cognitive System of Electromagnetic Spectrum Space (Nanjing University of Aeronautics and Astronautics), Ministry of Industry and Information Technology, Nanjing 211106, China*

Correspondence should be addressed to Yang Qian; qianyang@nuaa.edu.cn

Received 27 May 2022; Revised 23 July 2022; Accepted 30 July 2022; Published 20 September 2022

Academic Editor: Junpeng Shi

Direct position determination (DPD) of noncircular (NC) sources for multiple nested arrays (NA) is researched in this study. For noncircular sources, the dimension reduction method is used to decrease the computing complexity and remove the noncircular phase. Furthermore, nested array and noncircular sources extend spatial degree of freedom. Due to inferior stability and noise susceptibility of original algorithm, we propose SNR weighted subspace data fusion (W-SDF) algorithm. Each observation station places a nested array, spatial smoothing technology, and sum and difference co-array are used to deal with the nested array. Simulation results show that under nested array and noncircular sources, the proposed W-SDF algorithm has decreased the complexity of the algorithm and improved the location accuracy, degree of freedom, and resolution.

1. Introduction

In modern wireless location system, the focus of research is fast and accurate signal location [1]. The traditional positioning technology system is mostly a two-step estimation mode such as the correlation measurement, time difference of arrival (TDOA), frequency difference of arrival (FDOA), and energy gain. Therefore, location information is extracted from the signal data radiated by the target [2]. Then, the position parameters of the target are obtained from the above observations. The two-step positioning method has the characteristics of decentralization and does not need to transmit all signal data to the same central station for processing [3]. Therefore, it has low requirements for communication transmission bandwidth and calculation, which is convenient for engineering implementation [4]. From the positioning principle, the two-step positioning method is difficult to obtain the asymptotically optimal estimation accuracy, because it has experienced many processing links [5]. In addition, the two-step positioning is easy to lose the correlation of multiple stations, and the lost information is difficult to make up in the second-step positioning link [6]. In order to avoid the above problems, the direct position determination method is proposed. The core idea is to directly obtain the position information of the target from the original sampling signal without estimating the intermediate observation value. This principle avoids the problem of data association [7–10]. Therefore, direct positioning method has higher estimation accuracy and resolution [11–14].

Nowadays, there have been few reports about sparse array for direct determination position. In 2010, professor P. Pal proposed the nested array structure [15]. The nested array can greatly increase the degree of freedom of the array than the uniform linear array (ULA) [16–21]. In 2011, professor P. Pal proposed the coprime array structure, which is basically the same as the nested array structure. The obtained array degree of freedom is less than the nested array, but more sparse than the nested array [22]. J. Galy used the noncircular features of sources to increase the performance of DOA estimation. J. Galy proposed the MUSIC algorithm for noncircular sources, which pioneered

the application of noncircular sources in spatial spectrum estimation [23]. Yin applied the noncircular features of sources to direct positioning field with a moving array. The noncircular signal improves spatial degree of freedom and increases the positioning accuracy [24]. Zhang et al. applied the noncircular characteristics of sources to direct positioning with a moving coprime array [25]. At present, noncircular signal is rarely applied in direct positioning with multiple nested arrays [26–29]. Therefore, it is very important to study the noncircular sources for direct positioning with multiple nested arrays.

In this study, we use the noncircular sources characteristic to expand the spatial degree of freedom. The dimension method is used to decrease the computing complexity. In this study, the nested array is introduced into direct positioning. Therefore, array aperture is extended and the spatial smoothing method is adopted. Because the traditional SDF method is easily affected by noise and has inferior stability, the weighted SDF method is proposed [8]. Therefore, we can obtain high positioning accuracy.

The main contributions are as follows:

(1) We apply noncircular sources and the dimensionality reduction method to the direct location with noncircular sources to reduce the computational complexity and remove the phase of noncircular sources.

(2) We place a nested array on each observation station and use spatial smoothing technology and sum and difference co-array to deal with the nested array to expand the array aperture.

(3) We assign a weight to each station to improve the positioning accuracy because the SDF algorithm is vulnerable to noise and poor stability. Therefore, SNR weighted SDF loss function is set up.

The composition is as below. In Section 2, we expound on a direct position determination model, a common two-level nested array, and some notions about noncircular sources. In the next section, we depict spatial smoothing technology and SNR weighted SDF algorithm. In Section 4, we analyze the performance about the W-SDF algorithm and expound on its advantages from degree of freedom, computing complexity, and positioning accuracy. In Section 5, we emulate the weighted SDF algorithm and compare the performance of proposed algorithm with that of other algorithms. The last section summarizes this study.

Notations. $(\bullet)^H$, $(\bullet)^T$, and $(\bullet)^*$ mean conjugate transpose, transpose, and conjugate. The symbol $\otimes$ and $\mathrm{vec}(\bullet)$ mean the Kronecker product and matrix vectorization. I_n means an $n \times n$ unit matrix and $E(\bullet)$ means the mathematical expectation.

2. Preliminaries

In this section, we expound on a common two-level nested array and some notions about noncircular sources. Then, we describe multiple nested arrays combination direct positioning model.

2.1. Two-Level Nested Array Model. In Figure 1, the ordinary two-level nested array has $H = 6$ array elements, the dense uniform linear array (ULA) has $M = 3$ array elements, and the sparse array has $N = 3$ array elements. Uniform linear array element interval is $d_1 = d$, and sparse linear array element interval is $d_2 = 4d$, where $d = \lambda/2$, and λ expresses as signal wavelength. Figure 2 shows the positive sum co-array (a), the negative sum co-array (b), and difference co-array (c). Successive fictitious elements are placing from $-11d$ to $11d$.

2.2. Direct Position Determination Model. Direct position determination scenario is shown in Figure 3. Q independent narrow-band noncircular sources are in far-field X-Y plane. Multiple sources are $\mathbf{p}_q = [x_q, y_q]^T (q = 1, 2, \ldots Q)$. L nested arrays with $H = M + N$ array elements are placing at L stations $\mathbf{u}_l = [x_{ul}, y_{ul}]^T (l = 1, 2, \ldots, L)$.

The output signal of the $lth (l = 1, 2, \ldots, L)$ array at the $kth (k = 1, 2, 3 \ldots K)$ sampling snapshot time can be indicated as follows [9]:

$$\mathbf{r}_l(k) = \sum_{q=1}^{Q} \mathbf{a}_l\left(\mathbf{p}_q\right) f_{l,q}(k) + \mathbf{n}_l(k), \tag{1}$$

where $f_{l,q}(k)$ means the source waveform, $\mathbf{n}_l(k)$ means the noise vector for the lth station, and $\mathbf{a}_l(\mathbf{p}_q)$ means the orientation vector. This is all depending on the arrival direction orientation of the signal $\theta_l(\mathbf{p}_q)$ [9]:

$$\begin{aligned} \theta_l\left(\mathbf{p}_q\right) &= \arctan \frac{\mathbf{x}_{ul}(1) - \mathbf{p}_q(1)}{\mathbf{y}_{ul}(2) - \mathbf{p}_q(2)}, \\ \mathbf{a}_l\left(\mathbf{p}_q\right) &= \left[1, e^{-j2\pi d \sin\theta_l\left(\mathbf{p}_q\right)}, \ldots, e^{-j2\pi(H-1)d\sin\theta_l\left(\mathbf{p}_q\right)}\right]^T. \end{aligned} \tag{2}$$

Equation (1) can be indicated as follows [9]:

$$\mathbf{r}_l(k) = \mathbf{A}_l(\mathbf{p})\mathbf{f}_l(\mathbf{k}) + \mathbf{n}_l(k), \tag{3}$$

where

$$\begin{aligned} \mathbf{A}_l(\mathbf{p}) &= \left[\mathbf{a}_l(\mathbf{p}_1), \mathbf{a}_l(\mathbf{p}_2), \ldots, \mathbf{a}_l\left(\mathbf{p}_Q\right)\right], \\ \mathbf{f}_l(k) &= \left[f_{l,1}(k), f_{l,2}(k), \ldots, f_{l,Q}(k)\right]^T, \\ \mathbf{p} &= \left[\mathbf{p}_1^{\mathrm{T}}, \mathbf{p}_2^{\mathrm{T}}, \ldots, \mathbf{p}_Q^{\mathrm{T}}\right]^T, \\ \mathbf{n}_l(k) &= \left[\mathbf{n}_{l,1}(k), \mathbf{n}_{l,2}(k), \ldots, \mathbf{n}_{l,H}(k)\right]^T. \end{aligned} \tag{4}$$

2.3. Noncircular Sources Model. The sources studied in this study are noncircular sources. Reference [29] shows that any digital modulated signal $f(t)$ in the complex plane expression is obtained as follows:

$$f(t) = \sigma e^{-j\varphi}\left(\sqrt{\frac{1+k}{2}} f_1(t) + j\sqrt{\frac{1-k}{2}} f_Q(t)\right), \tag{5}$$

where φ is rotation phase, $k (0 \le k \le 1)$ controls signal amplitude, signal power $E\left\{\left|f(t)^2\right|\right\} = \sigma^2$, $f_1(t)$ and $f_Q(t)$ are

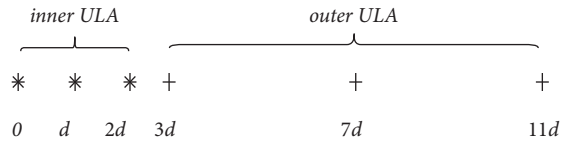

Figure 1: Two-level nested array.

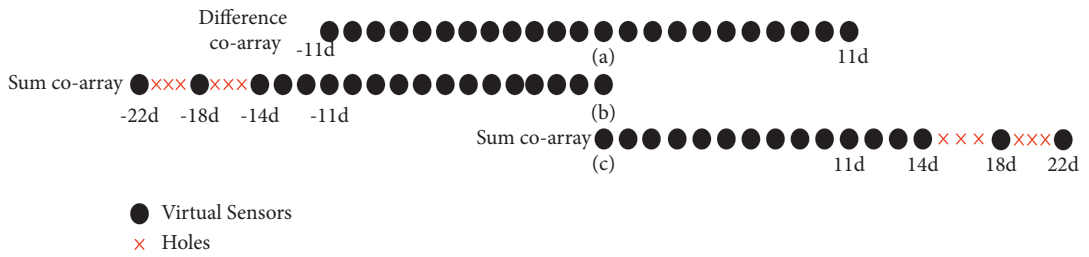

Figure 2: Difference co-array and sum co-array.

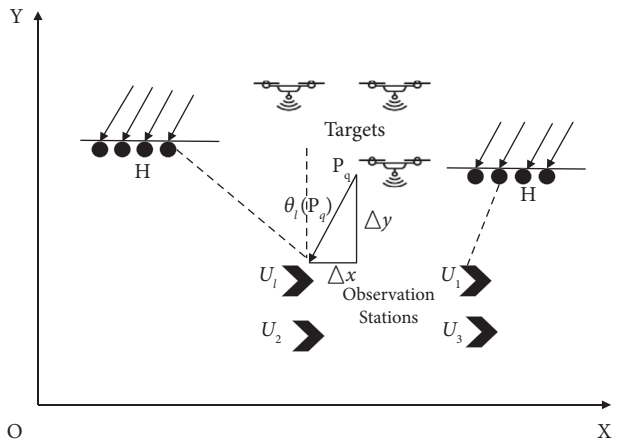

Figure 3: Multiple arrays combination positioning scene.

unit codirectional component and unit orthogonal component, satisfying $E\{|f_1(t)|^2\} = 1$, $E\{|f_Q(t)|^2\} = 1$, and $E\{f_1(t)f_Q(t)\} = 0$. When $k = 0$, the sources are called circular sources; when $k \neq 0$, the sources are called noncircular sources.

In order to measure the degree of noncircular for sources, literature [26–28] give the definition of noncircular sources:

$$E\left[\mathbf{f}_l(k)\mathbf{f}_l^{\mathbf{H}}(k)\right] = \rho e^{j\varphi} E\left[\mathbf{f}_l(k)\mathbf{f}_l^T(k)\right], \tag{6}$$

where φ denotes the noncircular phase, and ρ denotes the noncircular rate of the value in 0–1. In particular, when $\rho = 1$, the signal was called strictly noncircular sources.

According to reference [27], noncircular sources can be indicated as follows:

$$\mathbf{f}(t) = \mathbf{\Phi}\mathbf{f}^0(t), \tag{7}$$

where

$$\mathbf{\Phi} = \begin{bmatrix} e^{-j\varphi_1} & 0 & \dots & 0 \\ 0 & e^{-j\varphi_2} & \dots & . \\ . & . & . & . \\ 0 & . & 0 & e^{-j\varphi_Q} \end{bmatrix}, \tag{8}$$

where $\mathbf{f}^0(t)$ means the real part of the signal.

According to equation (7), equation (4) can be indicated as follows:

$$\mathbf{r}_l(k) = \mathbf{A}_l(\mathbf{p})\mathbf{\Phi}\mathbf{f}_l^0(k) + \mathbf{n}_l(k), \tag{9}$$

where

$$\mathbf{f}_l^0(k) = \left[f_{l,1}^{(0)}(k), f_{l,2}^{(0)}(k), \dots, f_{l,Q}^{(0)}(k)\right]^T. \tag{10}$$

3. The Proposed W-SDF Algorithm

In this section, we elaborate steps of weighted SDF algorithm, the process of spatial smoothing technology, and SNR weighting process.

3.1. Covariance Vectorization Signal. On the basis of the features of noncircular sources, we make use of dimension reduction method to decrease computational complexity and remove noncircular phase. We combine the SDF algorithm for direct position determination to obtain spectral peak search function.

We use features of noncircular sources to expand the received signal vector as follows [9]:

$$\mathbf{z}_l(k) = \begin{bmatrix} \mathbf{r}_1(k) \\ \mathbf{r}_1^*(k) \end{bmatrix} = \begin{bmatrix} \mathbf{A}_l(\mathbf{p})\mathbf{f}_l(k) \\ \mathbf{A}_l^*(\mathbf{p})\mathbf{f}_l^*(k) \end{bmatrix} + \begin{bmatrix} \mathbf{n}_l(k) \\ \mathbf{n}_l^*(k) \end{bmatrix}. \tag{11}$$

It can be obtained from equation (7):

$$\mathbf{f}_l^*(k) = \mathbf{\Phi}^*\mathbf{f}_l^{(0)}(k) = \mathbf{\Phi}^*\mathbf{\Phi}^{-1}\mathbf{f}_l(k) = \left(\mathbf{\Phi}^*\right)^2\mathbf{f}_l(k). \tag{12}$$

Then, equation (11) can be indicated as follows:

$$\begin{aligned}\mathbf{z}_l(k) &= \begin{bmatrix} \mathbf{A}_l(\mathbf{p}) \\ \mathbf{A}_l^*(\mathbf{p})\boldsymbol{\Phi}^*\boldsymbol{\Phi}^* \end{bmatrix}\mathbf{f}_l(k) + \begin{bmatrix} \mathbf{n}_l(k) \\ \mathbf{n}_l^*(k) \end{bmatrix} \\ &= \mathbf{C}_l(\mathbf{p})\mathbf{f}_l(k) + \begin{bmatrix} \mathbf{n}_l(k) \\ \mathbf{n}_l^*(k) \end{bmatrix},\end{aligned} \tag{13}$$

where

$$\%\ \mathbf{C}_l(\mathbf{p}) = \begin{bmatrix} \mathbf{A}_l(\mathbf{p}) \\ \mathbf{A}_l(\mathbf{p})\boldsymbol{\Phi}^*\boldsymbol{\Phi}^* \end{bmatrix} = \left[\mathbf{c}_l(\mathbf{p}_1), \mathbf{c}_l(\mathbf{p}_2), \ldots \mathbf{c}_l\left(\mathbf{p}_Q\right)\right], \tag{14}$$

where

$$\mathbf{c}_l\left(\mathbf{p}_q\right) = \begin{bmatrix} \mathbf{a}_l(\mathbf{p}) \\ \mathbf{a}_l(\mathbf{p})e^{j2\varphi_q} \end{bmatrix}. \tag{15}$$

The covariance matrix is as follows:

$$\begin{aligned}\mathbf{R}_l &= \frac{1}{K}\sum_{k=1}^{K}\mathbf{Z}_l(k)\mathbf{Z}_l^H(k) \\ &= \sum_{i=1}^{q}\sigma_{l,q}^2\mathbf{c}_l\left(\mathbf{p}_q\right)\mathbf{c}_l^H\left(\mathbf{p}_q\right) + \sigma_n^2\mathbf{I},\end{aligned} \tag{16}$$

where $\sigma_{l,q}^2$ means the power of the qth radiate source and σ_n^2 means noise power. For making use of features of nested array, we make the covariance matrix vector as follows [28]:

$$\begin{aligned}\mathbf{z}_l &= vec\left(\mathbf{R}_l\right) \\ &= vec\sum_{i}^{D}\sigma_{l,q}^2\mathbf{c}_l\left(\mathbf{p}_q\right)\mathbf{c}_l^H\left(\mathbf{p}_q\right) + \sigma_n^2\widetilde{I} \\ &= \mathbf{H}_l(\mathbf{p})\boldsymbol{\mu} + \sigma_n^2\widetilde{\mathbf{I}},\end{aligned} \tag{17}$$

where μ is the signal power vector and

$$\begin{aligned}\mathbf{H}_l(\mathbf{p}) &= \left[\mathbf{c}_l^*(\mathbf{p}_1)\otimes\mathbf{c}_l(\mathbf{p}_1), c_l^*(\mathbf{p}_2)\otimes\mathbf{c}_l(\mathbf{p}_2), \ldots, \mathbf{c}_l^*\left(\mathbf{p}_Q\right)\right. \\ &\quad \left.\otimes\mathbf{c}_l\left(\mathbf{p}_Q\right)\right], \\ \widetilde{\mathbf{I}} &= vec\left(\mathbf{I}_H\right),\end{aligned} \tag{18}$$

where

$$\begin{aligned}\left[\mathbf{c}_l^*\left(\mathbf{p}_q\right)\otimes\mathbf{c}_l\left(\mathbf{p}_q\right)\right] &= \begin{bmatrix} \mathbf{a}_l\left(\mathbf{p}_q\right) \\ \mathbf{a}_l^*\left(\mathbf{p}_q\right)e^{j2\varphi_q} \end{bmatrix}^* \otimes \begin{bmatrix} \mathbf{a}_l\left(\mathbf{p}_q\right) \\ \mathbf{a}_l^*\left(\mathbf{p}_q\right)e^{j2\varphi_q} \end{bmatrix} \\ &= \begin{bmatrix} \mathbf{a}_l^*\left(\mathbf{p}_q\right)\otimes\mathbf{a}_l\left(\mathbf{p}_q\right) \\ \mathbf{a}_l^*\left(\mathbf{p}_q\right)\otimes\mathbf{a}_l^*\left(\mathbf{p}_q\right)e^{j2\varphi_q} \\ \mathbf{a}_l\left(\mathbf{p}_q\right)\otimes\mathbf{a}_l\left(\mathbf{p}_q\right)e^{-j2\varphi_q} \\ \mathbf{a}_l\left(\mathbf{p}_q\right)\otimes\mathbf{a}_l^*\left(\mathbf{p}_q\right) \end{bmatrix} = \begin{bmatrix} p_1 \\ p_2 \\ p_3 \\ p_4 \end{bmatrix},\end{aligned} \tag{19}$$

where $p_1 = \mathbf{a}_l^*(\mathbf{p}_q)\otimes\mathbf{a}_l(\mathbf{p}_q)$, $p_2 = \mathbf{a}_l^*(\mathbf{p}_q)\otimes\mathbf{a}_l^*(\mathbf{p}_q)e^{j2\varphi_q}$, $p_3 = \mathbf{a}_l(\mathbf{p}_q)\otimes\mathbf{a}_l(\mathbf{p}_q)e^{-j2\varphi_q}$, and $p_4 = \mathbf{a}_l(\mathbf{p}_q)\otimes\mathbf{a}_l^*(\mathbf{p}_q)$. In Figure 4, the successive array elements of difference co-array are in range of $[-(M_1-1)d, (M_1-1)d]$, where $M_1 = MN + N, M = 4, N = 4$. DIFF I and DIFF II represent difference co-array. The successive array elements of sum co-array are in range of $[-(M_2-1)d, 0]$ and $[0, (M_2-1)d]$, where $M_2 = MN + M + N$. SUM I and SUM II represent sum co-array.

After the elements are sorted and duplicated according to the phase, the two vectors can be regarded as a direction vector of continuous difference co-array DCA:

$$\mathbf{c}_d\left(\mathbf{p}_q\right) = e^{-j2\pi U_d d\sin\theta_l\left(\mathbf{p}_q\right)/\lambda}, \tag{20}$$

where $U_d = \langle -R_1, R_1\rangle$, $R_1 = MN + N - 1$.

The equivalent received signal of DCA can be obtained as follows:

$$\mathbf{b}_d = \mathbf{H}_d\boldsymbol{\gamma} + \sigma_n^2\mathbf{u}, \tag{21}$$

where $\mathbf{H}_d = \left[\mathbf{c}_d(\mathbf{p}_1)\ \mathbf{c}_d(\mathbf{p}_2)\ \ldots\ \mathbf{c}_d(\mathbf{p}_Q)\right]$ is direction matrix of DCA. $\boldsymbol{\gamma}$ is equivalent incident signal vector. $\mathbf{u}$ is vector with only the middle $R_1 + 1$ elements of 1 and other elements of $\mathbf{u}$ are 0.

The elements are sorted and removed according to phase. After repetition, the direction vectors can be indicated as follows, respectively:

$$\begin{aligned}\mathbf{c}_s^-\left(\mathbf{p}_q\right) &= e^{-j2\pi U_s^- d\sin\theta_l\left(p_q\right)/\lambda}e^{j2\varphi_q}, \\ \mathbf{c}_s^+\left(\mathbf{p}_q\right) &= e^{-j2\pi U_d d\sin\theta_l\left(p_q\right)/\lambda}e^{-j2\varphi_q},\end{aligned} \tag{22}$$

where $U_s^- = \langle -R_3, R_2\rangle$, $R_2 = 0$, and $R_3 = MN + M + N - 1$.

The equivalent received sources of SCA I and the equivalent received sources of SCA II can be obtained as follows:

$$\begin{aligned}\mathbf{b}_s^- &= \mathbf{H}_s^-\boldsymbol{\gamma}, \\ \mathbf{b}_s^+ &= \mathbf{H}_s^+\boldsymbol{\gamma},\end{aligned} \tag{23}$$

where $\mathbf{H}_s^- = \left[\mathbf{c}_s^-(\mathbf{p}_1)\ \mathbf{c}_s^-(\mathbf{p}_2)\ \ldots\ \mathbf{c}_s^-(\mathbf{p}_Q)\right]$ is directional matrix of SCA I and $\mathbf{H}_s^+ = \left[\mathbf{c}_s^+(\mathbf{p}_1)\ \mathbf{c}_s^+(\mathbf{p}_2)\ \ldots\ \mathbf{c}_s^+(\mathbf{p}_Q)\right]$ is directional matrix of SCA II.

3.2. Spatial Smoothing Technology. Different from the traditional spatial smoothing of the full array, this section carries out the strategy of backward spatial smoothing for the continuous difference co-array DCA and the negative and positive semiaxis continuous sum co-array SCA I and SCA II respectively.

In Figure 4, for successive difference co-array DCA, we divide DCA into $R_1 + 1$ equivalent subarrays, which has $R_1 + 1$ elements each. The corresponding received signal can be indicated as follows [9]:

$$\mathbf{b}_{di} = \widetilde{\mathbf{H}}_d\boldsymbol{\Psi}^{i-1}\boldsymbol{\gamma} + \sigma_n^2\widetilde{\mathbf{u}}_i, \tag{24}$$

where b_{di} means $ith\,(i = 1, 2, \ldots, R_1 + 1)$ subarray, $\widetilde{\mathbf{u}}_i$ means the vector that the ith element value is 1, and the other element values are all 0 [9]. $\widetilde{\mathbf{H}}_d = [\widetilde{\mathbf{c}}_d(\mathbf{p}_1),$

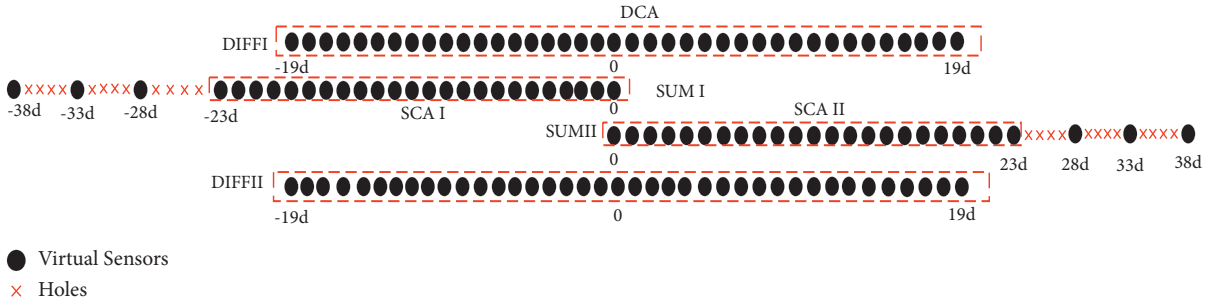

Figure 4: Array graph of sum and difference co-array.

$\tilde{\mathbf{c}}_d(\mathbf{p}_2), \ldots, \tilde{\mathbf{c}}_d(\mathbf{p}_q)]$ means the orientation matrix of SS-DCA, and its qth orientation vector can be indicated as follows [9]:

$$\tilde{\mathbf{c}}_d(\mathbf{p}_q) = \left[1, e^{-j\pi \sin\theta_l(\mathbf{p}_q)}, e^{-j2\pi \sin\theta_l(\mathbf{p}_q)}, \ldots, e^{-jR_1\pi \sin\theta_l(\mathbf{p}_q)}\right]^T, \tag{25}$$

$$\boldsymbol{\Psi} = diag\left\{e^{j\pi \sin\theta_l(\mathbf{p}_1)}, e^{j\pi \sin\theta_l(\mathbf{p}_2)}, \ldots, e^{j\pi \sin\theta_l(\mathbf{p}_Q)}\right\}. \tag{26}$$

The received sources of $R_1 + 1$ subarrays are connected together, and equation (26) shows received sources matrix after spatial smoothing $\mathbf{B}_d \in C^{(R_1+1)\times(R_1+1)}$:

$$\begin{aligned}\mathbf{B}_d &= \left[\mathbf{b}_{d1}, \mathbf{b}_{d2}, \ldots, \mathbf{b}_{d(R_1+1)}\right] \\ &= \tilde{\mathbf{H}}_d\left[\boldsymbol{\gamma}, \boldsymbol{\Psi}\boldsymbol{\gamma}, \ldots, \boldsymbol{\Psi}^{R_1}\boldsymbol{\gamma}\right] + \sigma_n^2 I_{R_1+1} \\ &= \tilde{\mathbf{H}}_d\tilde{\mathbf{S}} + \sigma_n^2\mathbf{I}_{R_1+1},\end{aligned} \tag{27}$$

where $\tilde{\mathbf{S}} = [\boldsymbol{\gamma}, \boldsymbol{\Psi}\boldsymbol{\gamma}, \ldots, \boldsymbol{\Psi}^{R_1}\boldsymbol{\gamma}]$, and $\mathbf{B}_d$ means the received sources of the first smooth subarray SS-DCA. Element location range of SS-DCA is $\langle 0, R_1\rangle$.

For successive sum co-array, they are divided into $R_1 + 1$ subarray. The number of elements of each subarray is $R_3 - R_2 - R_1 + 1$. After divided, the $ith (i = 1, 2, \ldots, R_1 + 1)$ received sources of the SCA I and received sources of SCA II are as follows [9]:

$$\begin{aligned}\mathbf{b}_{si}^- &= \widetilde{\mathbf{H}_s^-}\boldsymbol{\Psi}^{i-1}\boldsymbol{\gamma}, \\ \mathbf{b}_{si}^+ &= \widetilde{\mathbf{H}_s^+}\boldsymbol{\Psi}^{i-1}\boldsymbol{\gamma},\end{aligned} \tag{28}$$

where $\widetilde{\mathbf{H}_s^-} = [\tilde{\mathbf{c}}_s^-(\mathbf{p}_1), \tilde{\mathbf{c}}_s^-(\mathbf{p}_2), \ldots, \tilde{\mathbf{c}}_s^-(\mathbf{p}_q)]$, the array elements location range of SS-SCA I is $\langle -(R_3 - R_1), 0\rangle$, and the corresponding qth orientation vector can be indicated as follows:

$$\tilde{\mathbf{c}}_s^-(\mathbf{p}_q) = \left[e^{j(R3-R_1)\pi \sin\theta_l(\mathbf{p}_q)}e^{j2\varphi_q}, \ldots, e^{j\pi \sin\theta_l(\mathbf{p}_q)}e^{j2\varphi_q}, e^{j2\varphi_q}\right]^T, \tag{29}$$

where $\widetilde{\mathbf{H}_s^+} = [\tilde{\mathbf{c}}_s^+(\mathbf{p}_1), \tilde{\mathbf{c}}_s^+(\mathbf{p}_2), \ldots, \tilde{\mathbf{c}}_s^+(\mathbf{p}_q)]$, the array elements location range of SS-SCA II is $\langle R_1, R_3\rangle$, and the corresponding qth orientation vector can be indicated as follows:

$$\tilde{\mathbf{c}}_s^+(\mathbf{p}_q) = \left[e^{-jR_1\pi \sin\theta_l(\mathbf{p}_q)}e^{-j2\varphi_q}, e^{-j(R_1+1)\pi \sin\theta_l(\mathbf{p}_q)}e^{-j2\varphi_q}, \ldots, e^{-jR_3\pi \sin\theta_l(\mathbf{p}_q)}e^{-j2\varphi_q}\right]^T. \tag{30}$$

The received sources matrix of SS-SCA I and the received sources matrix of SS-SCA II are indicated as follows:

$$\begin{aligned}\mathbf{B}_s^- &= \left[\mathbf{b}_{s1}^-, \mathbf{b}_{s2}^-, \ldots, \mathbf{b}_{s(R_1+1)}^-\right] = \widetilde{\mathbf{H}_s^-}\tilde{\mathbf{S}}, \\ \mathbf{B}_s^+ &= \left[\mathbf{b}_{s1}^+, \mathbf{b}_{s2}^+, \ldots, \mathbf{b}_{s(R_1+1)}^+\right] = \widetilde{\mathbf{H}_s^+}\tilde{\mathbf{S}}.\end{aligned} \tag{31}$$

The received signal consists of $\mathbf{B}_s^-, \mathbf{B}_d, \mathbf{B}_s^+$, as shown in the following equation:

$$\tilde{\mathbf{B}} = \begin{bmatrix}\mathbf{B}_s^- \\ \mathbf{B}_d \\ \mathbf{B}_s^+\end{bmatrix} = \begin{bmatrix}\tilde{\mathbf{H}}_s^- \\ \tilde{\mathbf{H}}_d \\ \tilde{\mathbf{H}}_s^+\end{bmatrix}\tilde{S} + \begin{bmatrix}\mathbf{O}_{(R_3-R_1+1)\times(R_1+1)} \\ \sigma_n^2\mathbf{I}_{R_1+1} \\ \mathbf{O}_{(R_3-R_1+1)\times(R_1+1)}\end{bmatrix} = \tilde{\mathbf{H}}\tilde{\mathbf{S}} + \mathbf{U}, \tag{32}$$

where $\tilde{\mathbf{H}} = \left[\tilde{\mathbf{c}}(\mathbf{p}_1)\ \tilde{\mathbf{c}}(\mathbf{p}_2)\ \ldots\ \tilde{\mathbf{c}}(\mathbf{p}_q)\right]$ is direction matrix of SDCA, and SDCA denotes fictitious array after spatial smoothing and corresponding qth orientation vector can be indicated as follows:

$$\tilde{\mathbf{c}}(\mathbf{p}) = \begin{bmatrix}\tilde{\mathbf{c}}_s^- \\ \tilde{\mathbf{c}}_d \\ \tilde{\mathbf{c}}_s^+\end{bmatrix}. \tag{33}$$

As shown in Figure 5, a longer fictitious array is set up. There are 28 array elements after spatial smoothing, where $M = 4, N = 4$.

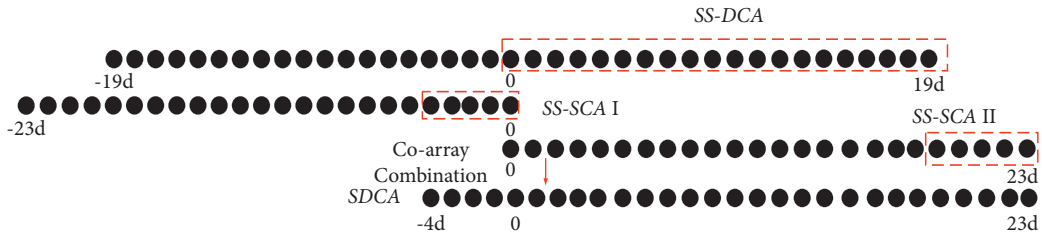

Figure 5: Nested array framework graph after spatial smoothing.

Firstly, the estimated value of the covariance matrix of the smoothed SDCA received signal is calculated as follows:

$$\mathbf{R}_Y = \frac{1}{\mathbf{R}_1 + 1}\widetilde{\mathbf{Y}}\widetilde{\mathbf{Y}^{\mathbf{H}}}. \tag{34}$$

The noise subspace $\mathbf{E}_l^n$ can be obtained by eigenvalue decomposition $\mathbf{R}_Y$. $(\mathbf{E}_l^n)^H\tilde{\mathbf{c}}(\mathbf{p}_q) = 0$, so cost function of noncircular sources is as follows:

$$f_{NC\text{-}S\,DF}(\mathbf{p},\varphi) = \arg\max \frac{1}{\sum_{l=1}^{L}\tilde{\mathbf{c}}(\mathbf{p},\varphi)^H\mathbf{E}_l^n(\mathbf{E}_l^n)^H\tilde{\mathbf{c}}(\mathbf{p},\varphi)}. \tag{35}$$

This study makes use of dimension reduction method to decrease the computational complexity and eliminate the noncircular phase. The qth direction is shown in the following equation:

$$\begin{aligned}\tilde{\mathbf{c}}(\mathbf{p}_q,\varphi_q) &= \begin{bmatrix} e^{j(R_3-R_1)\pi\sin\theta_l(\mathbf{p}_q)}e^{j2\varphi_q} \\ \cdot \\ \cdot \\ e^{j\pi\sin\theta_l(\mathbf{p}_q)}e^{j2\varphi_q} \\ \hline 1 \\ e^{-j\pi\sin\theta_l(\mathbf{p}_q)} \\ \cdot \\ \cdot \\ e^{-jR_1\pi\sin\theta_l(\mathbf{p}_q)} \\ \hline e^{-jR_1\pi\sin\theta_l(\mathbf{p}_q)}e^{-j2\varphi_q} \\ \cdot \\ \cdot \\ \cdot \\ e^{-jR_3\pi\sin\theta_l(\mathbf{p}_q)}e^{-j2\varphi_q} \end{bmatrix} = \begin{bmatrix} e^{j(R_3-R_1)\pi\sin\theta_l(\mathbf{p}_q)} & & & \\ \cdots & & & \\ e^{j\pi\sin\theta_l(\mathbf{p}_q)} & & & \\ 1 & & & \\ & 1 & & \\ & e^{-j\pi\sin\theta_l(\mathbf{p}_q)} & & \\ & \cdots & & \\ & e^{-jR_1\pi\sin\theta_l(\mathbf{p}_q)} & & \\ & & e^{-jR_1\pi\sin\theta_l(\mathbf{p}_q)} & \\ & & e^{-j(R_1+1)\pi\sin\theta_l(\mathbf{p}_q)} & \\ & & \cdots & \\ & & e^{-jR_3\pi\sin\theta_l(\mathbf{p}_q)} & \end{bmatrix} \begin{bmatrix} e^{j2\varphi_q} \\ 1 \\ e^{-j2\varphi_q} \end{bmatrix} \\ &= \boldsymbol{\Theta}(\mathbf{p}_q)\boldsymbol{\phi}(\varphi_q). \end{aligned} \tag{36}$$

Finally, we can obtain separation matrix $\boldsymbol{\phi}(\varphi_q) = \begin{bmatrix} e^{j2\varphi_q} & 1 & e^{-j2\varphi_q} \end{bmatrix}^T$. We set up $\mathbf{e} = \begin{bmatrix} 0 & 1 & 0 \end{bmatrix}^T$ to decrease searching dimension. So, it can eliminate noncircular phase. $\boldsymbol{\Theta}(\mathbf{p}_q)$ is another separation matrix.

Therefore, we can set up the cost function of RD-SDF algorithm as follows:

$$f_{RD\text{-}SDF}(\mathbf{p}) = \arg\max \sum_{l=1}^{L}\mathbf{e}^H\left(\boldsymbol{\Theta}^H(\mathbf{p})\mathbf{E}_l^n(\mathbf{E}_l^n)^H\boldsymbol{\Theta}(\mathbf{p})\right)^{-1}\mathbf{e}. \tag{37}$$

Because SDF only makes use of noise subspace, it is sensitive to external factors, such as few snapshots or low

signal-to-noise ratio. Therefore, we assign a weight to each observation station to improve positioning accuracy and set up the following cost function:

$$f_{W\text{-}S\ DF}(\mathbf{p}) = \arg\max \sum_{l=1}^{L} w_l e^H \left(\Theta^H(\mathbf{p})\mathbf{E}_l^n (E_l^n)^H \Theta(\mathbf{p})\right)^{-1} e, \tag{38}$$

where w_l means the weight of the lth station.

3.3. The Proposed SNR Weighted SDF. In view of the energy allocation principle on account of the water injection theory, the routes with good quality are distributed more power and the routes with poor quality are distributed less power. According to this principle, we can acquire the maximum route capacity. Due to inferior stability and noise susceptibility of ordinary algorithm, we propose SNR weighted method. For the sake of cutting down the total error, we devise a weight that increases as the error decreases.

Assuming that the noise is irrelevant and the sources and noise are mutually independent. Therefore, the covariance matrix can be reconstructed, and covariance matrix can be indicated as follows:

$$\widehat{\mathbf{R}}_l = \frac{1}{K}\sum_{k=1}^{K}\left(\sum_{q=1}^{Q}\mathbf{g}_{l,q}^2 W_q \mathbf{b}_l(\mathbf{p})\mathbf{b}_l^H(\mathbf{p}) + \sigma_n^2 \mathbf{I}_{V\times V}\right), \tag{39}$$

where $\mathbf{I}_{V\times V}$ is unit matrix of $V \times V$, where $V = MN + N$. The power of different emitter sources in the same array or different arrays in the same emitter source is decided by the sources power W_q and unknown parameters $g_{l,q}$.

Received sources covariance matrix are separated into two sections [8]:

$$\begin{aligned}\widehat{\mathbf{R}}_l &= \mathbf{R}_s + \mathbf{R}_n = \mathbf{A}_l(\mathbf{p})diag\left(\left[W_{l,1},\ldots,W_{l,Q}\right]\right)\mathbf{A}_l^H(\mathbf{p}) \\ &\quad + \sigma_n^2 \mathbf{I}_{V\times V}.\end{aligned} \tag{40}$$

Therefore, the eigenvalue can be indicated as follows [8]:

$$\lambda_{l,i} = \begin{cases} \sigma_{y_i}^2 + \sigma_n^2, & 1 \le i \le Q, \\ \sigma_n^2, & Q+1 \le i \le V, \end{cases} \tag{41}$$

where $\sigma_{y_i}^2, 1 \le i \le Q$ are Q eigenvalues of $\mathbf{R}_s$, and we use them represent the power of the received sources. According to equation (41), the estimated noise power can be obtained for the lth observation station as follows:

$$\widehat{\sigma}_{nl}^2 = \frac{1}{V-Q}\sum_{i=Q+1}^{V}\lambda_{l,i}. \tag{42}$$

According to (42), we can get the power of the lth station as below

$$\widehat{W}_l = \sum_{i=1}^{Q}\left(\lambda_{l,i} - \widehat{\sigma}_{nl}^2\right). \tag{43}$$

The received signal with large signal-to-noise ratio will engender smaller position error. So, we should distribute larger weight to the location. The cost function is set up as follows:

$$f_{SW\text{-}SDF}(\mathbf{p}) = \arg\max \sum_{l=1}^{L}\frac{\widehat{W}_l}{\widehat{\sigma}_{nl}^2}\mathbf{e}^H\left(\mathbf{\Theta}^H(\mathbf{p})\mathbf{a}_j^H(\mathbf{p})\mathbf{E}_l^n(\mathbf{E}_l^n)^H(\mathbf{p})\mathbf{a}_j\mathbf{\Theta}(\mathbf{p})^{-1}\mathbf{e}\right). \tag{44}$$

Through searching the Q minimum values of equation (44), we can get the estimated location.

3.4. The Steps of the W-SDF Algorithm. We make a list of the following 5 steps about W-SDF algorithm. Figure 6 shows the flowchart of the algorithm.

Step 1. Establish a direct positioning scene model.

Step 2. For the nested array, we use the spatial smoothing method and the sum difference array method to get a larger array aperture.

Step 3. Calculate the covariance matrix and get the noise subspace.

Step 4. Generate the weighting coefficient w_l and use the dimension reduction method to set up the loss function $f_{SW\text{-}SDF}(\mathbf{p})$.

Step 5. Obtain the value of spectral peak through spectral peak search, which is the corresponding coordinate $(\hat{x}_q, \hat{y}_q)$.

4. Performance Analysis

In this section, the available DOF and the complexities of the W-SDF, SDF, Capon, and W-Capon algorithms are analyzed. Finally, we elaborate the advantages of W-SDF algorithm.

4.1. Achievable DOFs. We define that M means the number of dense uniform subarray, N means the number of sparse subarray, and H means the whole number of array elements. After spatial smoothing, the DOF of W-SDF algorithm is $MN + 2M + N$. DOF of proposed algorithm for circular sources with uniform linear subarray is H, DOF of proposed algorithm for noncircular sources with uniform linear subarray is $2H$, and DOF for circular sources with nested array is $MN + N$. It is obviously that the DOF has increased a lot.

4.2. Complexity Analysis. We define that H means numbers of array element, Q means numbers of source, L means numbers of observation station, and K means numbers of snapshots. The X orientation is separated into L_x equivalent

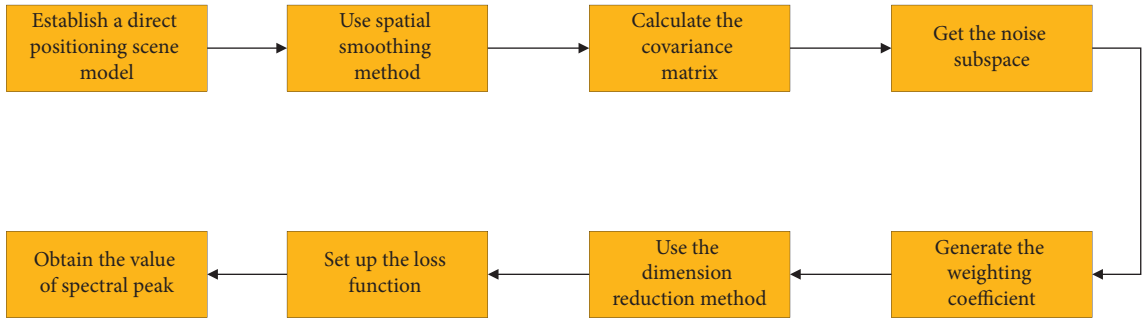

Figure 6: Algorithm flowchart.

portions, and Y orientation is separated into L_y equivalent portions [10]. Noncircular phase is separated into L_φ equivalent portions. The computer configuration is Intel(R) Core i7-10700F, and CPU frequency is 2.90 GHz.

The computing complexity for DPD mainly includes four portions: the complexity of covariance matrix is $O(4H^2LK)$, the computing complexity of covariance after spatial smoothing is $O[F^2VL]$, where $F = MN + M + 2N$, $V = MN + N$. The eigenvalue decomposition of the covariance matrix is $O[F^3L]$, and the computing complexity of spatial spectral peak searching value after SNR weighting is $O[LL_xL_y(3F^2 + 9F + F^2(F - Q) + 39]$. Table 1 lists the computing complexity of the W-SDF, SDF, Capon, and W-Capon algorithms and running time of these algorithms.

The W-SDF algorithm of computational complexity without dimension reduction is $O[4M^2LK + F^2VL + F^3L + LL_xL_yL_\varphi(F^2 + F + F^2(F - Q))]$.

The W-SDF algorithm of computational complexity with dimension reduction is $O[4M^2LK + F^2VL + F^3L + LL_xL_y(3F^2 + 9F + F^2(F - Q) + 39)]$.

It is obviously that the computational complexity is lessened after dimension reduction.

It can be seen from Figure 7 that W-SDF has the same computational complexity as the SDF algorithm and W-Capon has the same complexity as the Capon algorithm. W-SDF has lower computational complexity compared with W-Capon and Capon algorithm.

4.3. Advantages. We expound on the advantages about the proposed method from degree of freedom, computing complexity, and positioning accuracy.

(1) The proposed method makes use of noncircular sources and nested array features to expand aperture. The degree of freedom has been greatly improved.

(2) We make use of dimension reduction method to decrease computational complexity of algorithms for noncircular sources. The computing complexity is obviously lessened.

(3) We integrate the weighting method into SDF and obtain high accuracy. We make use of noncircular sources and nested arrays and get higher positioning accuracy.

5. Simulation Results

In this section, we emulate the proposed method and get the pattern of spatial spectrum and scatter diagram. We emulate the RMSE results of the proposed method under different parameters.

5.1. Estimated Results Concerning Proposed Method. Multiple nested arrays are located at multiple targets $\mathbf{P}_1 = [300m, 300m]$, $\mathbf{P}_2 = [500m, 500m]$, and $\mathbf{P}_3 = [800m, 800m]$. The noncircular phase is $(\pi/6, \pi/4, \pi/3)$. The observation stations are $\mathbf{U}_1 = [-2000m, -100m]$, $\mathbf{U}_2 = [-1000m, -100m]$, $\mathbf{U}_3 = [0m, -100m]$, $\mathbf{U}_4 = [1000m, -100m]$, and $\mathbf{U}_5 = [2000m, -100m]$. Figure 8 shows pattern of spatial spectrum and Figure 9 shows scatter diagram of three targets. The real location and estimated location are shown in Figure 8. The proposed W-SDF algorithm can locate three source targets accurately.

The location estimation performance is analyzed through computing Monte Carlo (MC) simulation times. The root mean squares error (RMSE) can be indicated as follows [9]:

$$RMSE = \frac{1}{Q}\sum_{q=1}^{Q}\sqrt{\frac{1}{MC}\sum_{mc=1}^{MC}\left[\left(\hat{x}_{q,mc} - x_q\right)^2 + \left(\hat{y}_{q,mc} - y_q\right)^2\right]}, \tag{45}$$

where MC means the number of Monte Carlo experiment times, Q means the number of targets, (x_q, y_q) means the true location of the qth target source, and $(\hat{x}_{q,mc}, \hat{y}_{q,mc})$ means the estimated position for the qth target in the $mcth$ experiment. We set Monte Carlo simulation times as 500.

5.2. Performance of W-SDF and SDF Algorithms under Different Sources and Arrays. Multiple targets are $\mathbf{P}_1 = [300m, 300m]$, $\mathbf{P}_2 = [500m, 500m]$, and $\mathbf{P}_3 = [800m, 800m]$. The number of snapshots is 300. The number of nested array element is $(M, N) = (3, 3)$. Figure 10 shows the performance of SDF algorithm and W-SDF algorithm under noncircular sources with different arrays. Figure 10 also shows that the performance of SDF algorithm and W-SDF algorithm for different sources under uniform linear array. The performance of weighted SDF algorithm is superior to SDF algorithm. The performance of SDF and

Table 1: Computing complexity and working time.

Different algorithms	Computing complexity	Working time (s)
SDF	$O[4M^2LK + F^2VL + F^3L + LL_xL_y(3F^2 + 9F + F^2(F-Q) + 39)]$	145.378111
W-SDF	$O[4M^2LK + F^2VL + F^3L + LL_xL_y(3F^2 + 9F + F^2(F-Q) + 39)]$	146.294961
Capon	$O[4M^2LK + F^2VL + LL_xL_y(3F^2 + 9F + F^3 + 39)]$	1360.93077
W-Capon	$O[4M^2LK + F^2VL + LL_xL_y(3F^2 + 9F + F^3 + 39)]$	1369.73693

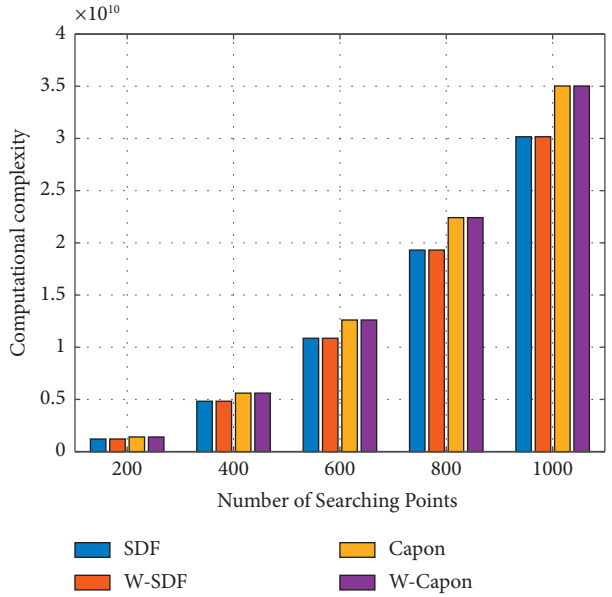

Figure 7: Computational complexity of different algorithms.

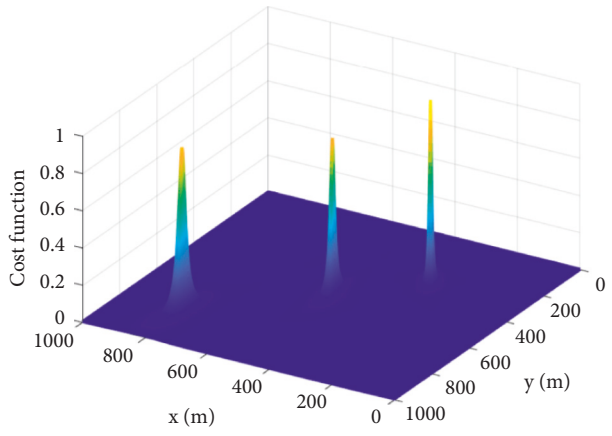

Figure 8: Multiple targets direct position.

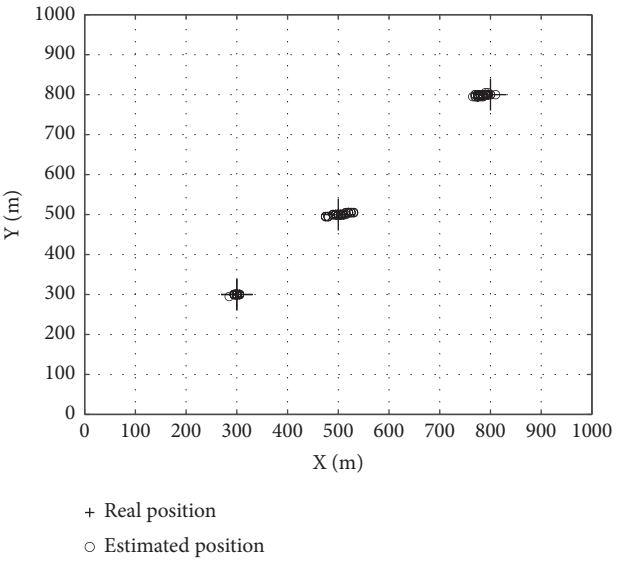

Figure 9: Scatter diagram of three targets.

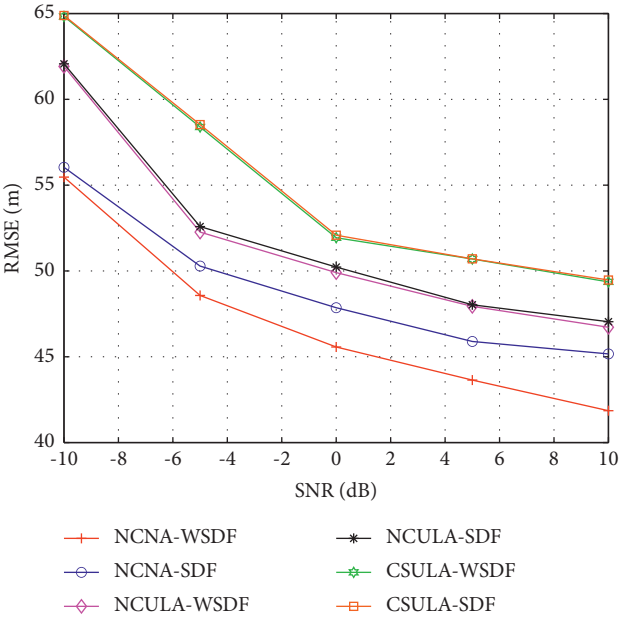

Figure 10: W-SDF and SDF algorithms for different arrays and sources.

W-SDF algorithms for noncircular sources is superior to that of circular sources. The performance of SDF and W-SDF algorithms for nested array is superior to that of uniform linear array.

5.3. Performance of Different Algorithms for Noncircular Sources. The number of snapshots is 300. Multiple targets are $\mathbf{P}_1 = [300m, 300m]$, $\mathbf{P}_2 = [500m, 500m]$, and $\mathbf{P}_3 = [800m, 800m]$. The number of nested array element is $(M, N) = (3, 3)$. Figure 11 shows the performance of W-SDF, SDF, W-Capon, Capon, and W-PM and PM algorithms under nested arrays and noncircular sources. Under noncircular sources and nested array, the performance of the W-SDF algorithm is superior to W-Capon and

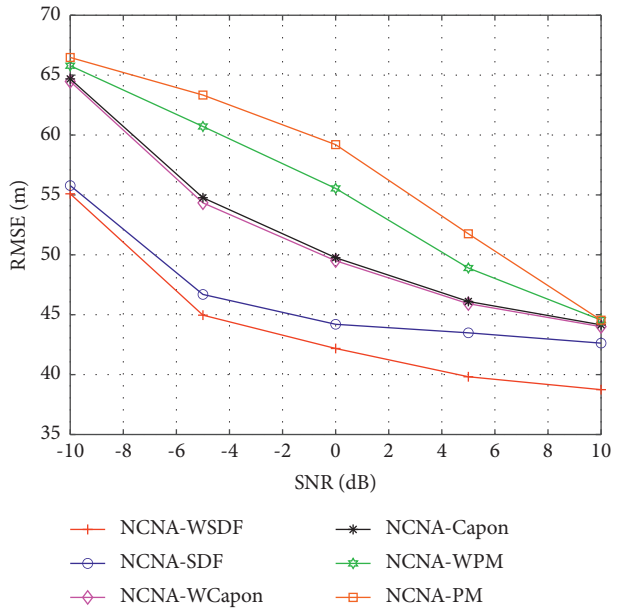

Figure 11: Different algorithms comparison for noncircular sources.

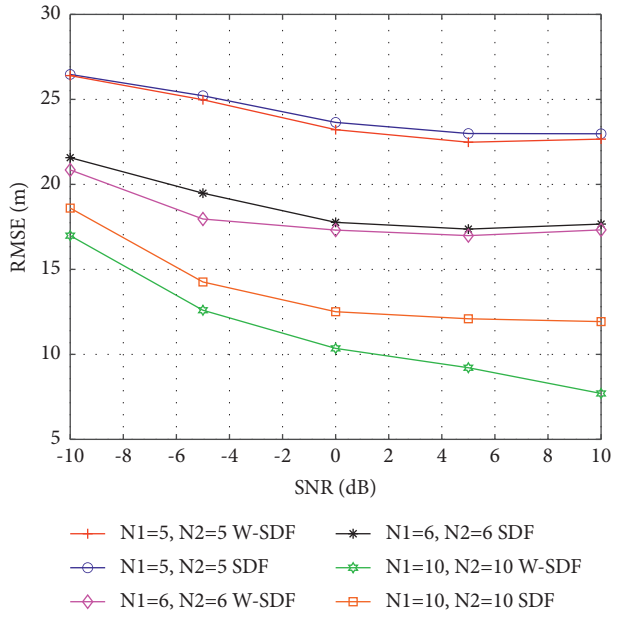

Figure 12: W-SDF and SDF algorithms for different element numbers.

W-PM algorithms. The performance of W-SDF algorithm is superior to SDF, Capon, and PM algorithm.

5.4. Performance of W-SDF and SDF Algorithms with Increment of Array Element Numbers. Multiple targets are $\mathbf{P}_1 = [300m, 300m]$, $\mathbf{P}_2 = [500m, 500m]$, and $\mathbf{P}_3 = [800m, 800m]$. The number of snapshots is 300. Figure 12 shows the performance of W-SDF and SDF under nested array $(M, N) = (5, 5), (6, 6), (10, 10)$. With the

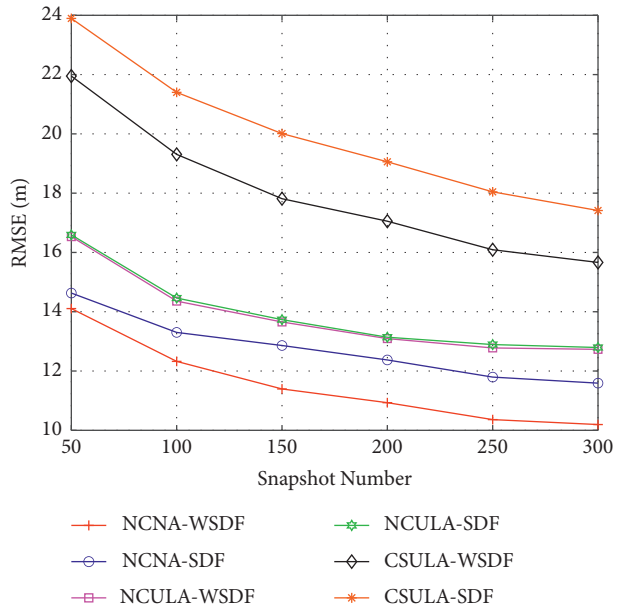

Figure 13: W-SDF and SDF algorithms with different snapshot numbers.

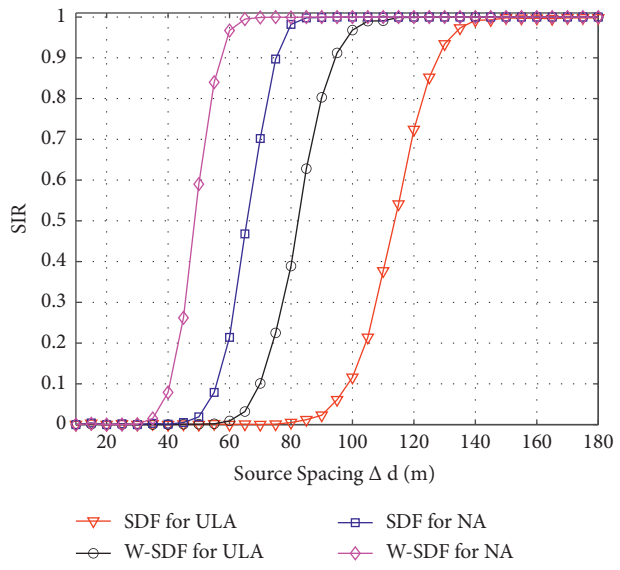

Figure 14: Resolution about W-SDF and SDF algorithms.

number of array elements increment, the performance of SDF and W-SDF for nested array and noncircular sources is better.

5.5. Performance of W-SDF and SDF Algorithms with Different Snapshot Numbers. Figure 13 shows the performance of SDF and W-SDF algorithms under different number of snapshots. Multiple targets are $\mathbf{P}_1 = [300m, 300m]$, $\mathbf{P}_2 = [500m, 500m]$, and $\mathbf{P}_3 = [800m, 800m]$. The SNR is set as 15 dB. The nested array element number is $(M, N) = (3, 3)$. With the increment of snapshot number, it

is clearly to see that the performance for nested arrays and noncircular sources is better.

5.6. Resolution about Source Spacing with Different Arrays. Figure 14 shows resolution about the distance between two sources. SNR is set as 5 dB. Positions are set as $\mathbf{p}_1 = [300m, 300m]$ and $\mathbf{p}_2 = [\Delta dm, 300m]$, where Δd changes from 10 m to 180 m. It can be seen that the resolution of weighted SDF algorithm is better than that of SDF algorithm with noncircular sources, and the resolution of algorithm under nested array is better than that under uniform array.

6. Conclusion

This article studies SNR weighted SDF algorithm on account of noncircular sources and nested arrays for direct position determination. For noncircular sources, the dimension reduction method is used to decrease the computing complexity and remove the noncircular phase. For SDF algorithm vulnerable to noise and inferior stability, we use SNR weighted SDF algorithm to improve location accuracy. For the aperture limited, we introduce nested arrays to expand array aperture. We use spatial smoothing technology and use sum and difference co-array to deal with the nested array. Simulation results show that the proposed method decreases the complexity of the algorithm and improves the location accuracy, degree of freedom, and resolution. In the future, we can study an optimal station position. Three-level nested arrays and other sparse arrays for the direct positioning are also needed researched in the future.

Data Availability

The data used to support the findings of this study are included within the article.

Conflicts of Interest

The authors declare that they have no conflicts of interest.

Acknowledgments

This work was supported by the China NSF (Grant nos. 61971217, 61971218, and 61631020), Jiangsu NSF (Grant no. BK20200444), Suzhou Key Research and Development Project(Grant no. SGC2021069), and National Key Research and Development Project, (Grant no. 2020YFB1807602).

References

[1] Y. Wang and Y. Wu, "An efficient semidefinite relaxation algorithm for moving source localization using TDOA and FDOA measurements," *IEEE Communications Letters*, vol. 21, no. 1, pp. 80–83, 2017.

[2] Y. Xie, Y. Wang, P. Zhu, and X. You, "Grid-search-based hybrid TOA/AOA location techniques for NLOS environments," *IEEE Communications Letters*, vol. 13, no. 4, pp. 254–256, 2009.

[3] T. Qiao, Y. Zhang, and H. Liu, "Nonlinear expectation maximization estimator for TDOA localization," *IEEE Wireless Communications Letters*, vol. 3, no. 6, pp. 637–640, 2014.

[4] F. Wen, Q. Wan, and L. Y. Luo, "Time-difference-of-arrival estimation for noncircular signals using information theory," *AEU-International Journal of Electronics and Communications*, vol. 67, no. 3, pp. 242–245, 2013.

[5] Q. Liu, J. Xu, Z. Ding, and H. C. So, "Target localization with jammer removal using frequency diverse array," *IEEE Transactions on Vehicular Technology*, vol. 69, no. 10, pp. 11685–11696, 2020.

[6] O. Bialer, D. Raphaeli, and A. J. Weiss, "Maximum-likelihood direct position estimation in dense multipath," *IEEE Transactions on Vehicular Technology*, vol. 62, no. 5, pp. 2069–2079, 2013.

[7] K. Hao and Q. Wan, "High resolution direct detection and position determination of sources with intermittent emission," *IEEE Access*, vol. 7, pp. 43428–43437, 2019.

[8] Y. Qian, Z. Yang, and H. Zeng, "Direct position determination for augmented coprime arrays via weighted subspace data fusion method," *Mathematical Problems in Engineering*, vol. 2021, pp. 1–10, Article ID 2825025, 2021.

[9] Y. Qian, D. Zhao, and H. Zeng, "Direct position determination of noncircular sources with multiple nested arrays: reduced dimension subspace data fusion," *Wireless Communications and Mobile Computing*, vol. 2021, pp. 1–10, Article ID 9950518, 2021.

[10] X. Shi, X. Zhang, and H. Zeng, "Direct position determination of non-circular sources for multiple arrays via weighted euler ESPRIT data fusion method," *Applied Sciences*, vol. 12, no. 5, 2022.

[11] F. Ma, Z. M. Liu, and F. Guo, "Direct position determination in asynchronous sensor networks," *IEEE Transactions on Vehicular Technology*, vol. 68, no. 9, pp. 8790–8803, 2019.

[12] T. Zhou, W. Yi, and L. Kong, "Direct position determination of multiple coherent sources using an iterative adaptive approach," *Signal Processing*, vol. 161, pp. 203–213, 2019.

[13] J. Yin, D. Wang, and Y. Wu, "An efficient direct position determination method for multiple strictly noncircular sources," *Sensors*, vol. 18, no. 2, p. 324, 2018.

[14] Y. K. Zhang, H. Y. Xu, B. Ba, D. M. Wang, and W. Geng, "Direct position determination of non-circular sources based on a Doppler-extended aperture with a moving coprime array," *IEEE Access*, vol. 6, pp. 61014–61021, 2018.

[15] P. Pal and P. P. Vaidyanathan, "Nested arrays: a novel approach to array processing with enhanced degrees of freedom," *IEEE Transactions on Signal Processing*, vol. 58, no. 8, pp. 4167–4181, 2010.

[16] Y. Wang, W. Wu, X. Zhang, and W. Zheng, "Transformed nested array designed for DOA estimation of non-circular signals: reduced sum-difference Co-array redundancy perspective," *IEEE Communications Letters*, vol. 24, no. 6, pp. 1262–1265, 2020.

[17] C. L. Liu and P. P. Vaidyanathan, "Super nested arrays: linear sparse arrays with reduced mutual coupling–part I: fundamentals," *IEEE Transactions on Signal Processing*, vol. 64, no. 15, pp. 3997–4012, 2016.

[18] W. Si, Z. Peng, C. Hou, and F. Zeng, "Improved nested arrays with sum-difference co array for DOA estimation," *IEEE Sensors Journal*, vol. 19, no. 16, pp. 6986–6997, 2019.

[19] P. Gupta and M. Agrawal, "Design and analysis of the sparse array for DOA estimation of noncircular signals," *IEEE Transactions on Signal Processing*, vol. 67, no. 2, pp. 460–473, 2019.

[20] J. Shi, F. Wen, and T. Liu, "Nested MIMO radar: coarrays, tensor modeling and angle estimation," *IEEE Transactions on Aerospace and Electronic Systems*, vol. 57, no. 1, pp. 573–585, 2021.

[21] M. Yang, L. Sun, X. Yuan, and B. Chen, "Improved nested array with hole-free DCA and more degrees of freedom," *Electronics Letters*, vol. 52, no. 25, pp. 2068–2070, 2016.

[22] P. P. Vaidyanathan and P. Pal, "Sparse sensing with coprime samplers and arrays," *IEEE Transactions on Signal Processing*, vol. 59, no. 2, pp. 573–586, 2011.

[23] P. Gounon, C. Adnet, and J. Galy, "Location angulaire de signaux non circulares," *Traitement du Signal*, vol. 15, no. 1, pp. 17–23, 1998.

[24] J. X. Yin, Y. Wu, and D. Wang, "Direct position determination of multiple noncircular sources with a moving array," *Circuits, Systems, and Signal Processing*, vol. 36, no. 10, pp. 4050–4076, 2017.

[25] Y. Zhang, B. Ba, D. Wang, W. Geng, and H. Xu, "Direct position determination of multiple non-circular sources with a moving coprime array," *Sensors*, vol. 18, no. 5, p. 1479, 2018.

[26] J. Liu, Z. Huang, and Y. Zhou, "Extended 2q-MUSIC algorithm for noncircular signals," *Signal Processing*, vol. 88, no. 6, pp. 1327–1339, 2008.

[27] B. Picinbono, "On circularity," *IEEE Transactions on Signal Processing*, vol. 42, no. 12, pp. 3473–3482, 1994.

[28] Y. Wang, J. Shen, X. Zhang, Y. He, and X. Dai, "Noncircular signals for nested array: sum-difference co-array and DOA estimation algorithm," *IET Radar, Sonar & Navigation*, vol. 14, no. 1, pp. 27–35, 2019.

[29] J. Steinwandt, F. Roemer, and M. Haardt, "ESPRIT-type algorithms for a received mixture of circular and strictly noncircular signals," *IEEE International Conference on Acoustics, Speech and Signal Processing*, vol. 14, no. 1, pp. 2809–2813, 2015.